ELSEVIER

Available online at www.sciencedirect.com
ScienceDirect
Journal of Hydrodynamics
2008,20(2):154-163

www.sciencedirect.com/
science/journal/10016058

AN INVESTIGATION OF TURBULENT RECTANGULAR JET DISCHARGED INTO A NARROW CHANNEL WEAK CROSSFLOW*

PATHAK Manabendra, DASS Anoop K., DEWAN Anupam
Department of Mechanical Engineering, Indian Institute of Technology Guwahati, Guwahati – 781039, India,
E-mail: manabendra.pathak@gmail.com

(Received October 8, 2007, Revised November 8, 2007)

Abstract: A computational investigation of the mean flow field of turbulent rectangular jets issuing into a narrow channel crossflow is presented. The length of the jet slot spans more than 55% of the crossflow channel bed, leaving a small clearance between the jet edge and sidewalls. A finite volume code employing the standard k-ε model is used to predict the mean, three-dimensional flow field. The mean flow field is investigated for two velocity ratios (6 and 9). Important flow features, such as the formation of different vortical structures and their characteristics owing to different values of the velocity ratio, are discussed. Some predicted results are compared with the experimental data reported in the literature. The predicted mean and turbulent flow properties are shown to be in good agreement with the experimental data.

Key words: turbulent jet, crossflow, narrow channel, velocity ratio, vortices

1. Introduction

The problem of turbulent jets in crossflow is observed in several engineering and environmental issues. Owing to its enormous applications, the flow configuration of a jet in a crossflow has been studied extensively both experimentally and computationally during the past several decades. Even though extensive studies of the problem have been carried out in the past several decades, some aspects of the flow field have not been investigated in detail. One of these aspects is the jet in a narrow channel crossflow, i.e., the case where the distance between the two sidewalls is relatively small thus leaving a small clearance between the jet edge and sidewalls. We present here the results from the investigation of the flow structures that form owing to the interaction of the jet with a narrow channel crossflow.

The flow field of jets in crossflow is quite complex as it is characterized by the streamline curvature effects [1-3] and by the formation of different types of vortices owing to the interactions of the jet and crossflow. Four types of vortices are observed in the flow field, namely, (1) roll-up in the jet shear layer vortices, (2) Counter-Rotating Vortex Pair (CRVP), (3) a horse-shoe vortex system, and (4) the wake vortices[4,5] .

The main parameter that characterizes the flow field of jet in crossflow is the jet-to-crossflow velocity ratio, $R=v_j/u_a$ or the momentum flux ratio $J=\rho_j R^2/\rho_a$, where, v_j and u_a are the velocity of jet and crossflow, respectively, and ρ_j and ρ_a are the corresponding densities. Depending on the value of R, the flow regime can change. Lim [6] observed that at a high velocity ratio ($R > 2$), the jet penetrates significantly into the crossflow and it bends over far enough downstream of the injection hole. Therefore, for these types of jets, there is little influence of the bottom wall on its development. Moreover, there is a little effect of the crossflow boundary layer characteristics on the flow for high values of R, as the jet is able to penetrate through a relatively thin

* **Biography:** PATHAK Manabendra (1970-), Male, Ph. D.
Corresponding Author: DEWAN Anupam,
E-mail: adewan@iitg.ernet.in

boundary-layer. On the other hand, for low velocity ratios, i.e., $R < 1$, the jet bends over into the wall at a small downstream distance and then it spreads over the wall. There is no wake region downstream of the jet injection hole and the jet behaves like a wall jet. For $1 \le R \le 2$, the jet seems to be in an intermediate regime, in which it can reattach to the injection wall.

It is observed from the literature review that most studies on jets in crossflow are concerning the circular jet geometry and few literatures exist that deal with the non-circular (square, rectangular, or elliptic) geometry. Several researchers [7, 8] have found that the structure of the flow field of square jets in crossflow is nearly identical to the flow field of round jet in crossflow. Haven [9] pointed out that higher-aspect ratio jets have lower trajectories, partly owing to the decreased degree of interaction between the counter-rotating vortex-pairs.

The present study addresses two important issues of jet in crossflow: (1) jets in a narrow channel crossflow, and (2) rectangular jets with high velocity ratios (6 and 9), where the jet flow is strong compared to the crossflow. The flow configuration of the present investigation corresponds to the experimental work of Ramaprian [10] and Haniu [11] who performed the measurements of mean and turbulent flow properties in the central plane of the rectangular jet for the velocity ratio of R = 6, 9, and 10. They did not provide any details of the flow properties near the bottom wall and in transverse planes of the channel and did not resolve different vortical structures of the flow field. The objective of the present investigation is: (a) to provide more detailed information about the flow field of a rectangular jet discharged into a narrow channel crossflow with relatively high velocity ratio and (b) to study the effect of the velocity ratio on the flow field.

2. Mathematical formulations

A schematic diagram of the three-dimensional (3-D) computational domain and the co-ordinate system used in the present study is shown in Fig.1. The size of the computational domain used depends upon the value of the jet to the crossflow velocity ratio (R). The sizes of the computational domain (Fig.1) used for different values of R are shown in Table 1.

2.1 *Governing equations*

The 3-D, steady-state, Reynolds-averaged Navier-Stokes equations for the incompressible flow form the governing equations, which may be expressed in the Cartesian tensor notation as follows:

Continuity:

$$\frac{\partial}{\partial x_j}\left(u_j\right) = 0 \tag{1}$$

Momentum:

$$\frac{\partial}{\partial x_j}\left(u_i u_j\right) = -\frac{\partial p}{\rho \partial x_i} + \frac{\partial}{\partial x_j}\left(-\overline{u_i' u_j'}\right) \tag{2}$$

Here, u_i denote the mean velocities and p denotes the mean pressure. The molecular viscosity is neglected except in the near wall region. The jet discharge and the flow in the entire computational domain are assumed to be fully turbulent and thus independent of the value of the Reynolds number.

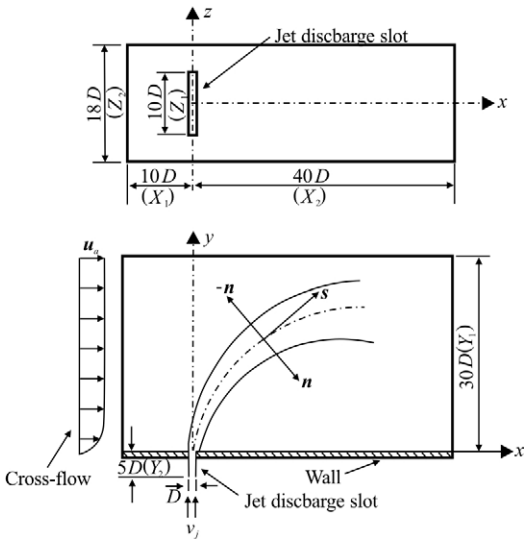


Fig.1 Schematic diagram of the computational domain for R = 6

2.2 *Turbulence model*

The governing Eqs. (1) and (2) require closure for the Reynolds stress tensor $\overline{u_i' v_j'}$, which is obtained by the standard k-ε model. In the standard k-ε model, the Reynolds stresses are modeled as

$$-\overline{u_i' v_j'} = \nu_t\left(\frac{\partial u_i}{\partial x_j} + \frac{\partial u_j}{\partial x_i}\right) - \frac{2}{3}k\delta_{ij} \tag{3}$$

where the eddy-viscosity is modeled as

Table 1 Domain size for different values of *R*

R	X_1 (*x*/*D*)	X_2 (*x*/*D*)	Y_1 (*y*/*D*)	Y_2 (*y*/*D*)	Z_1 (*z*/*D*)	Z_2 (*z*/*D*)
6	10	40	30	5	10	18
9	10	50	40	5	10	18

$$\nu_t = C_\mu \frac{k^2}{\varepsilon} \tag{4}$$

The turbulent kinetic energy (k) and dissipation rate (ε) in the flow field are determined from the solution of their individual transport equations. The transport equations for turbulence kinetic energy (k) and its dissipation rate (ε) used are as follows

$$u\frac{\partial k}{\partial x}+v\frac{\partial k}{\partial y}+w\frac{\partial k}{\partial z}=\frac{\partial}{\partial x}\left(\frac{\nu_t}{\sigma_k}\frac{\partial k}{\partial x}\right)+\frac{\partial}{\partial y}\bullet$$

$$\left(\frac{\nu_t}{\sigma_k}\frac{\partial k}{\partial y}\right)+\frac{\partial}{\partial z}\left(\frac{\nu_t}{\sigma_k}\frac{\partial k}{\partial z}\right)+P_k-\varepsilon \tag{5}$$

$$u\frac{\partial \varepsilon}{\partial x}+v\frac{\partial \varepsilon}{\partial y}+w\frac{\partial \varepsilon}{\partial z}=\frac{\partial}{\partial x}\left(\frac{\nu_t}{\sigma_\varepsilon}\frac{\partial \varepsilon}{\partial x}\right)+\frac{\partial}{\partial y}\bullet$$

$$\left(\frac{\nu_t}{\sigma_\varepsilon}\frac{\partial \varepsilon}{\partial y}\right)+\frac{\partial}{\partial z}\left(\frac{\nu_t}{\sigma_k}\frac{\partial \varepsilon}{\partial z}\right)+C_{\varepsilon 1}\frac{\varepsilon}{k}P_k-$$

$$C_{\varepsilon 2}\frac{\varepsilon^2}{k} \tag{6}$$

where P_k is the rate of production of k and is given by

$$P_k=\nu_t[(\frac{\partial u}{\partial y}+\frac{\partial v}{\partial x})^2+(\frac{\partial v}{\partial z}+\frac{\partial w}{\partial y})^2+$$

$$(\frac{\partial u}{\partial z}+\frac{\partial w}{\partial x})^2+2(\frac{\partial u}{\partial x})^2+2(\frac{\partial v}{\partial y})^2+2(\frac{\partial w}{\partial z})^2]$$

All parameters in Eqs. (1) to (6) are non-dimensionalized with the mean jet velocity v_j and jet width D as follows.

$$u^*=\frac{u}{v_j},\ v^*=\frac{v}{v_j},\ w^*=\frac{w}{v_j}$$

$$x^*=\frac{x}{D},\ y^*=\frac{y}{D},\ z^*=\frac{z}{D}$$

$$p^*=\frac{p}{\rho v_j^2},\ k^*=\frac{k}{v_j^2},\ \varepsilon^*=\frac{\varepsilon}{v_j^3/D}$$

2.3 *Boundary conditions*

The different boundary conditions used are inlet, outlet, and wall. At the inlet, the boundary conditions correspond to the crossflow conditions, i.e., the only component of the flow is along the crossflow direction ($u = u_a$) with zero components along both the vertical ($v = 0$) and spanwise directions ($w = 0$). The inlet boundary layer thickness is set to 1.5D to match the experimental conditions. Inside the boundary layer, the 1/7th power-law profile is used for the u-velocity component and a uniform velocity ($u = u_a$) is imposed above y =1.5D. The value of the turbulent kinetic energy at the left boundary is taken from 5% turbulent intensity based on the experimental data ($k = 0.00375u_a^2$). The inlet turbulence dissipation rate is obtained from the expression suggested by Versteeg [12] as $\varepsilon = c_\mu^{3/4}(k^{1/2}/y_{\max})$, where, $y_{\max}$ is the domain size in the y direction**.** At the top surface excluding the sidewall top, the free-stream condition is imposed and the values of k and ε specified are the same as those at the inlet boundary. The top of the sidewalls is treated as the wall. At the outlet plane, the normal gradients of all variables are assumed to be zero $\left(\partial f/\partial x = 0, f = u, v, w, k, \varepsilon\right)$. The whole bottom surface, excluding the jet discharge slot, is considered as a solid wall. The no slip condition is applied there and the standard wall functions are used to resolve the

near wall turbulence. The value of y^+ is taken as 11.3, above which the log-law is assumed to be valid. The boundary conditions at the entry to the jet channel or jet plenum are $u = 0$, $w = 0$, and $v = v_j$. The value of turbulent kinetic energy is taken from 6.5% turbulent intensity. Both the sidewalls are treated with the no-slip condition and the standard wall functions are used to resolve the near wall turbulence.

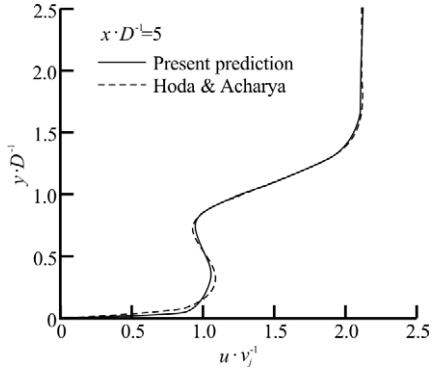


Fig.2 Comparison of the present predictions with those of Hoda [14] for velocity ratio of R= 0.5, z/D = 0

3. Numerical procedure

Non-uniform staggered grids are used in the present study. The grids are clustered at the jet exit region in the x-direction, near the bottom wall in the y-direction, and near both sidewalls in the z-direction. The grid sizes of the computations are fixed after a grid independent study. A grid size of 122×90×60= 658800 control volumes (122 along the x-direction, 90 along the y-direction, and 60 along the z-direction) is used for R = 6 and 142×104×70= 1033760 for R = 9. The governing equations and other transport equations are discretized using the power-law scheme [13]. The tri-diagonal matrix algorithm with line-by-line iteration process is used to solve the system of linear algebraic equations. For good convergence, an alternation of sweeping direction is done. All variables (u, v, w, k and ε) are under-relaxed during each iteration. The convergence of the computation is assumed to be achieved and therefore iterations are terminated when the normalized sum of the residual mass is less than 10^{-4} and the variation of the variables u, v, w, k and ε is less than 10^{-2} in their successive iterations. The code was run on a special Linux server (16 nodes, load clustering machine, 8 GB RAM, and 3 GHz processor speed) with serial computation and it took approximately 26 d of the CPU time for the full convergence of the results. For testing the accuracy of the present code, it was validated with the numerical results reported by Hoda [14] for a square jet in a crossflow for velocity ratio of R = 0.5. A comparison of the predicted results of the cross-stream components of the mean velocity at a location of x/D = 5, z/D = 0 for the velocity ratio R = 0.5 obtained by the present code with the results of Hoda [14] is shown in Fig.2. It is observed that the agreement between the two predictions is fairly good and the maximum difference between the two predictions is seen to be less than 5%.

4. Results and discussion

The computations are performed in the Cartesian coordinates and the computed data are subsequently transformed to the s–n co-ordinates (s- along the streamline and n- normal to it, Fig.1) for the purpose of comparison with the experimental data [10, 11].

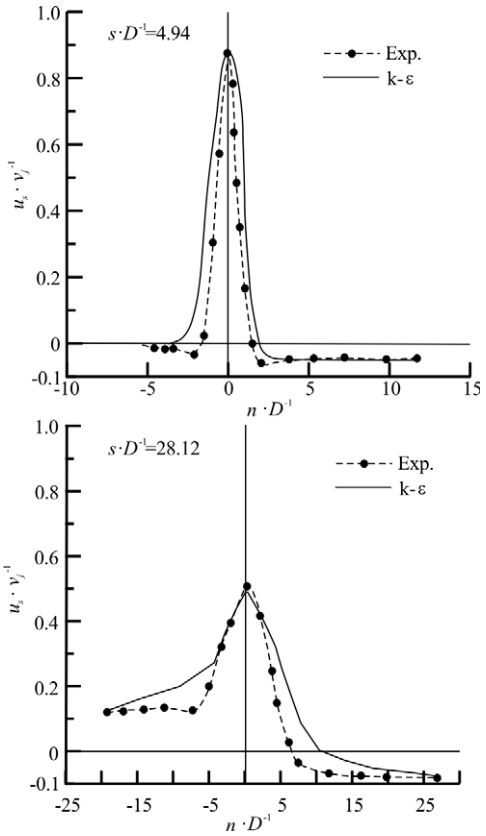


Fig.3 Comparison of mean streamwise velocity at the jet central plane (z/D = 0) for R = 6, s/D = 4.94 and 28.12

4.1 *Comparison with measurements*

A comparison of the normalized streamwise component of mean velocity (u_s/v_j) at the jet central vertical plane (z/D = 0) at two different downstream locations (s/D = 4.94 and 28.12) with the experimental data for the velocity ratio R = 6 is shown in Fig.3. The overall agreement of the predictions by the models at the locations of s/D = 4.94 is better than that at the far downstream positions of s/D = 28.12. The first position is in the vicinity of the jet exit region where

experimental conditions are used as the boundary conditions in the numerical predictions. At far downstream, the present computations overpredict the jet spread in the upper and the lower parts of the jet. At downstream positions, the jet is characterized with recirculation and streamline curvature effects. Therefore, at these locations, the agreement between the computational predictions and experimental results is not as good as in the near field. Moreover, the positions of the peak values do not match with the experimental data.

A comparison of the normalized *s*-component profiles of the mean velocity (u_s/v_j) at the jet central vertical plane (z/D = 0) at two different downstream locations (s/D = 4.97 and 29.73) with the experimental data for the velocity ratio R = 9 is shown in Fig.4. The agreement with the experimental data is better in the upper and lower parts of the jet at all s/D locations compared to the case with R = 6.

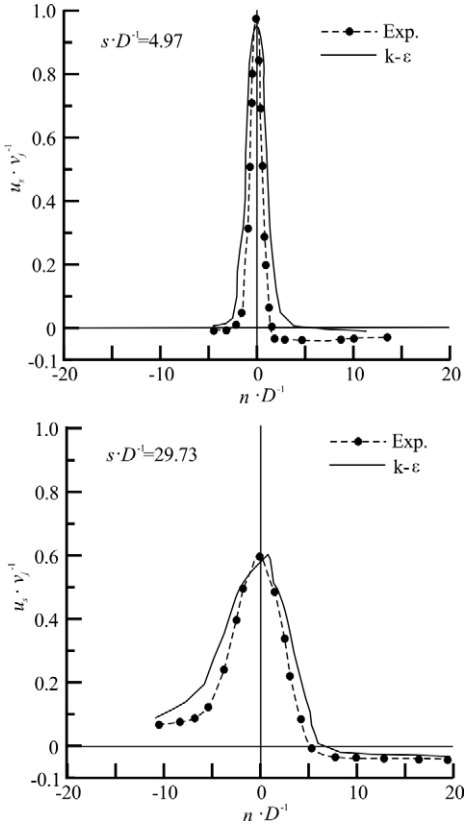


Fig.4 Comparison of the mean streamwise velocity at the jet central plane (z/D = 0) for R = 9, s/D = 4.97 and 29.73

4.2 *Component of mean velocity*

We have seen from the previous section that the present predictions are in reasonably good agreement with the experimental results. To gain an understanding of the flow physics in a clear way and to provide the flow properties near the bottom wall,we have presented the predictions of the mean flow properties in the Cartesian coordinates in this section.

Figures 5 and 6 show the variation of the cross-stream component of mean velocity (u/v_j) with distance y/D from the wall at various downstream positions (x/D) and at two different transverse planes for the velocity ratio R = 6. In Fig.5, the velocity profile at the jet central plane (z/D = 0) is shown. A reverse flow region is formed near the wall, just at the downstream of the jet (x/D = 2). A weak wall-jet-like structure at the positions of x/D = 5 and 10 is observed near the bottom wall. Since the crossflow is weak in this case, the wall-jet-like structure is weak compared to the case of strong crossflow, i.e., low values of the velocity ratio R [14, 15]). A wake region with a low velocity is observed above the wall-jet shear layer and a shear layer with strong velocity gradient above the wake region is observed at the locations of x/D = 2, 5, and 10.

Figure 6 shows the profiles at z/D = 6. The profiles at all downstream locations are expectedly different from those at the central plane (z/D = 0). The vertical height where the jet peak value occurs is less in this plane (z/D = 6) compared to that at the central plane. Near the bottom wall, the wall-jet shear layer is prominent at all downstream locations and it is formed even at x/D = 0 with steep velocity gradients.

The cross-stream components of the mean velocity profile at two different transverse planes (z/D = 0 and 6) and at different downstream locations (x/D = 0, 2, 5, 10 and 20) for the velocity ratio R = 9 are shown in Figs.7 and 8. The peak values of the cross-stream components are seen at higher values of y/D in this case compared to the case of the jet with R = 6. Thus, the jet penetrates more into the crossflow compared to the case with the velocity ratio R = 6. In this case also, the velocity profiles show weak wall-jet shear structures, wake region, and jet shear layer structures.

Figure 9 shows the downstream development of the vertical component (v/v_j) of the mean velocity in the jet central plane (z/D = 0) for R = 6. At the jet discharge point (x/D = 0), the vertical component of the velocity is largely unaffected by the crossflow up to the height of about y/D = 3, until which point, the jet is almost straight. After a certain height, the jet is deflected and therefore the value of the vertical velocity component reduces. At x/D = 2, the wake-like region starts at approximately y/D = 3 and moves away from the bottom wall as one goes in the downstream direction. Further downstream, the jet becomes almost horizontal and runs parallel to the crossflow. As there is no existence of the vertical jet, the values of the vertical components are quite small at those locations.

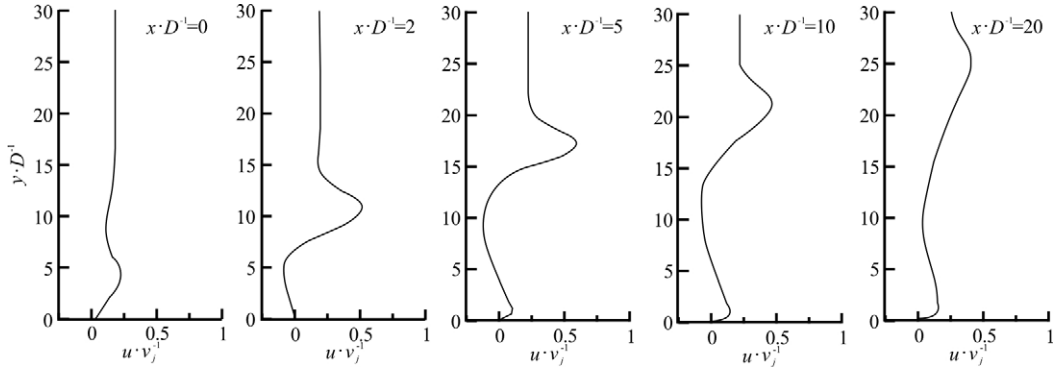


Fig.5 Predictions of cross-stream component of mean velocity at different downstream locations (z/D = 0) for R = 6

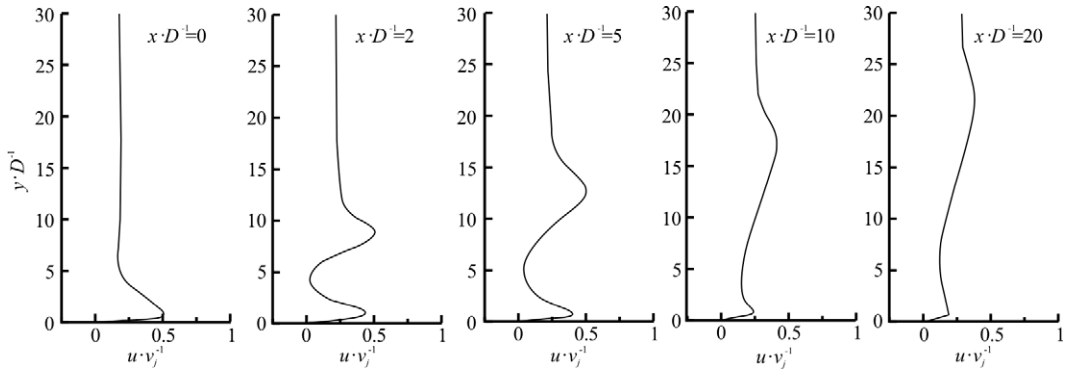


Fig.6 Predictions of cross-stream component of mean velocity at different downstream locations (z/D = 6) for R = 6

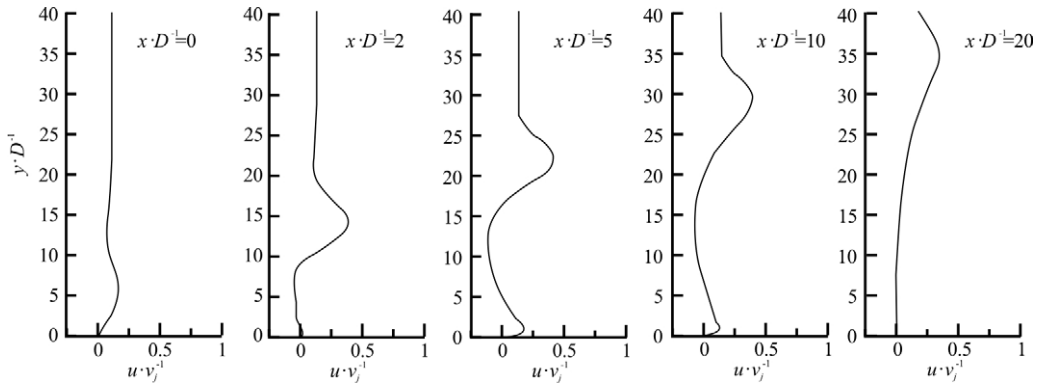


Fig.7 Predictions of cross-stream component of mean velocity at different downstream locations (z/D = 0) for R = 9

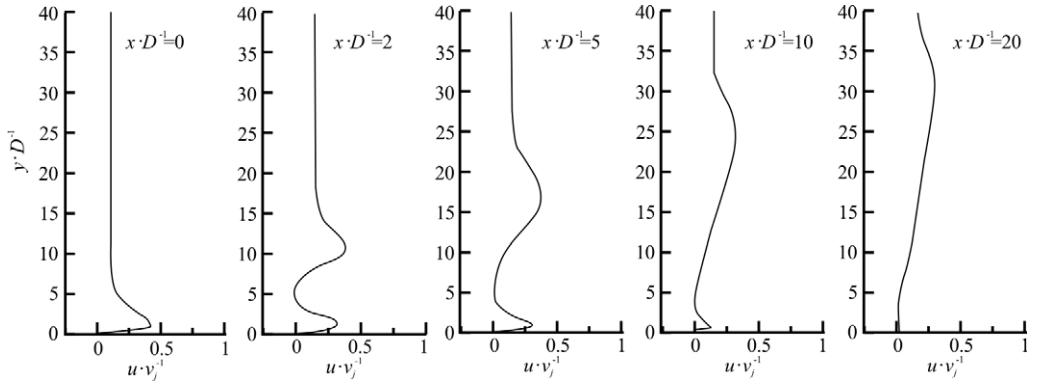


Fig.8 Predictions of cross-stream component of mean velocity at different downstream locations (z/D = 6) for R = 9

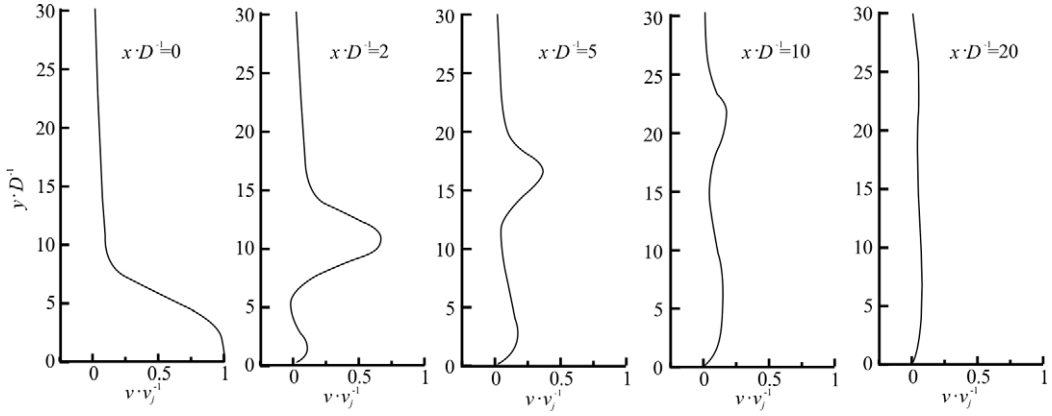


Fig.9 Predictions of vertical component of mean velocity at different downstream locations (z/D = 0) for R = 6

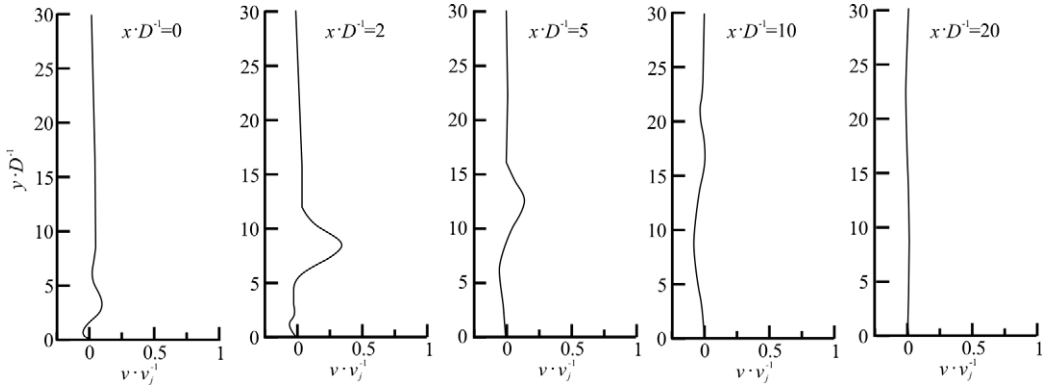


Fig.10 Predictions of vertical component of mean velocity at different downstream locations (z/D = 6) for R = 6

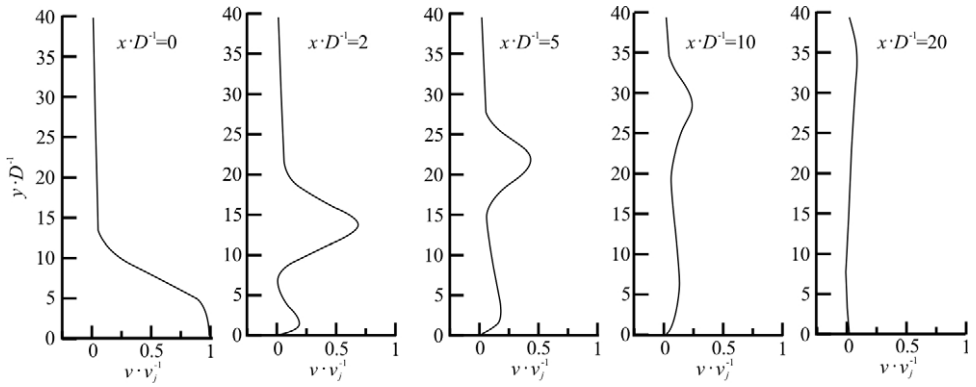


Fig.11 Predictions of vertical component of mean velocity at different downstream locations (z/D = 0) for R = 9

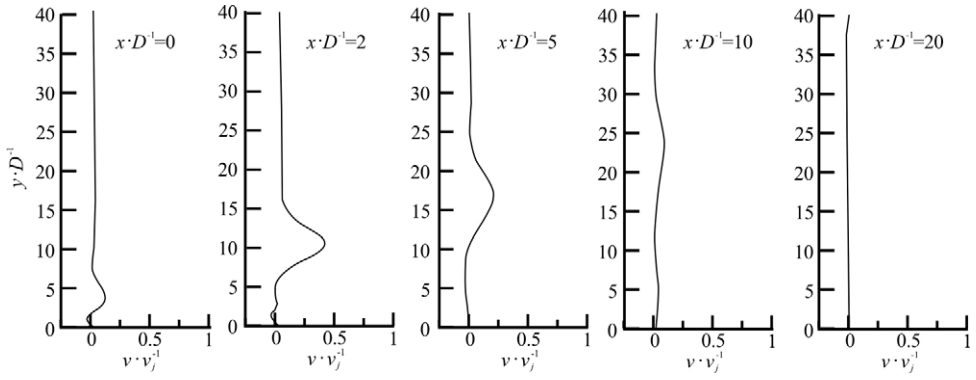


Fig.12 Predictions of vertical component of mean velocity at different downstream locations (z/D = 6) for R = 9

The changes of the vertical component profile at other transverse plane (z/D = 6) are shown in Fig.10. The velocity gradients $(\partial v/\partial y)$ in the wall-jet layer are observed to be smaller and the negative velocity in the wake region is reduced as one moves from the centre of the jet towards the sidewalls. The influence of the jet is limited up to a small downstream location (x/D = 5). The effect of the sidewalls on the flow is observed here.

Figures 11 and 12 show the vertical component of the mean velocity at different transverse planes and at different downstream locations for the velocity ratio R = 9. Qualitatively, the velocity profiles are similar to the case of R = 6 (Figs. 9 and 10).

Since the jet is comparatively strong in this case, the component of the vertical velocities shows a high value, and thus, the jet trajectory is larger in this case compared to the case with R = 6. The velocity gradient $\partial v/\partial y$ near the bottom wall at all downstream positions at z/D = 0 is observed to be less compared to the case with R = 6.

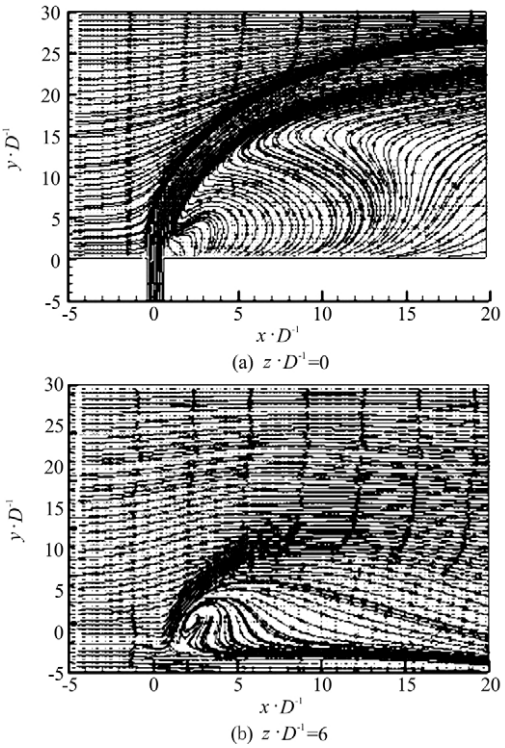


Fig.13 Mean x-y vector plots superimposed on streamlines at different spanwise locations for R = 6, z/D = 0 and 6

4.3 *Mean flow structures and their characteristics*

The predicted non-dimensional mean velocity vectors superimposed with the streamline plot at two different x-y planes in the spanwise direction for the velocity ratio R = 6 are shown in Fig.13. The two planes chosen are the jet discharge central plane (z/D = 0) and the plane at z/D = 6. At the jet central plane (z/D = 0), the jet trajectory is deflected in the cross-stream direction and the direction of the crossflow is altered as if an obstacle blocks it. However, owing to the effect of the jet entrainment and the motion of the jet, the flow field of a jet in crossflow is not exactly the same as that over a rigid obstacle. A wake region with a complex flow pattern is formed in the lee side of the jet. Very close to the bottom wall, a reverse flow region is formed and the cross-stream fluid is observed to enter this region. It is also observed that the structures and extent of the reverse flow regions downstream of the jet are different at the other plane (z/D = 6), thereby demonstrating the three-dimensionality of the flow.

Figure 14 shows the predicted non-dimensional mean velocity vectors superimposed on the streamlines at two different x-y planes in the spanwise direction for the velocity ratio R = 9. In this case, the jet trajectory is different from that in the case with R = 6. The undisturbed length of the jet is more in this case and the jet penetration into the crossflow is more compared to the case with R = 6.

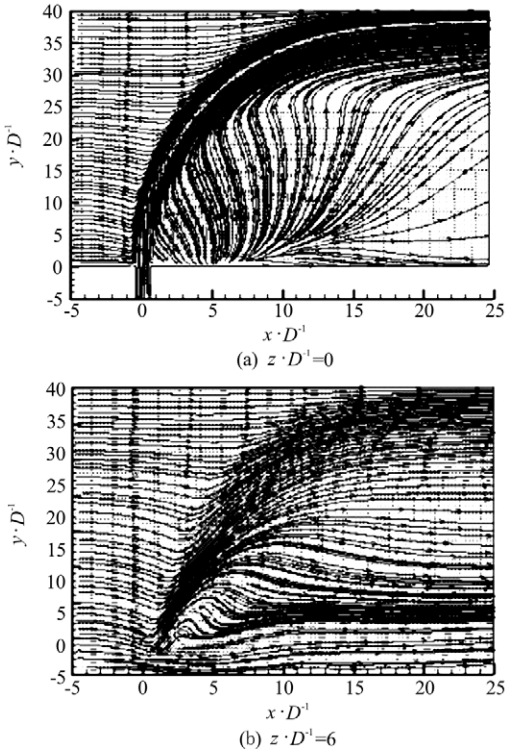


Fig.14 Mean x-y vector plots superimposed on streamlines at different spanwise locations for R = 9, z/D = 0 and 6

An interesting effect of the velocity ratio on the flow field is observed in the size of the reverse flow region. For the velocity ratio R = 9, the length of the reverse flow zone is decreased by as much as three slot widths or over 20% compared to that for the velocity ratio R = 6. In this case also, the flow pattern

at other spanwise plane (z/D = 6) is different from the flow pattern at the jet central plane (z/D = 0).

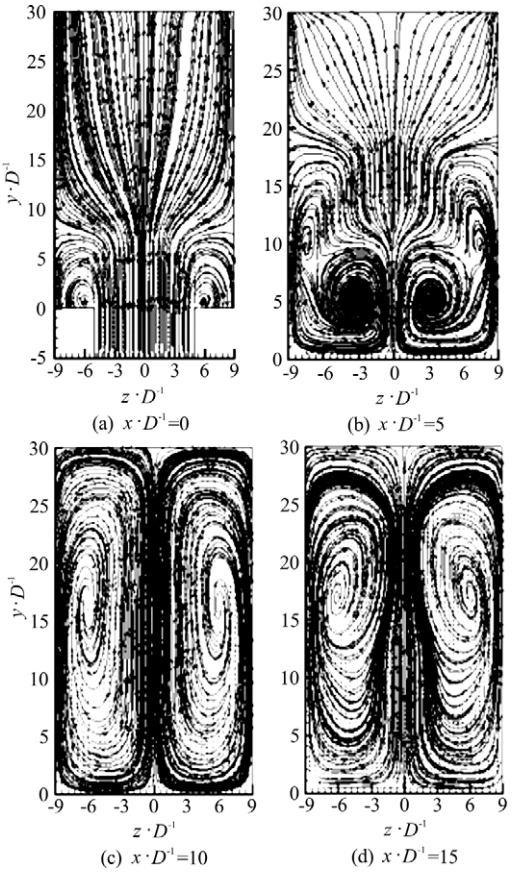


Fig.15 Mean *y-z* vector plots superimposed on streamline at different downstream locations for R = 6, x/D = 0, 5, 10, and 15

Figure 15 shows the mean velocity field at different *y-z* planes at various downstream locations (x/D = 0, 5, 10, and 15) for the velocity ratio R = 6. The inception of two vortices at both sides of the jet edge is observed at x/D = 0. Downstream of the jet slot (x/D = 5), the vortices produced at the side edge start to weaken and the two vortices formed at each side of the slot central plane start to enlarge. The continued development of the CRVP, which grows larger in size, is observed at the planes x/D = 10 and 15, respectively. The size of the vortex pair at the plane x/D = 10 becomes very large. The pressure drop in the wake region induces an inward motion, transporting the fluid from the crossflow towards the jet central plane. The development of the CRVP appears to be full fledged at x/D = 15, which grows in size and assumes the shape of a kidney.

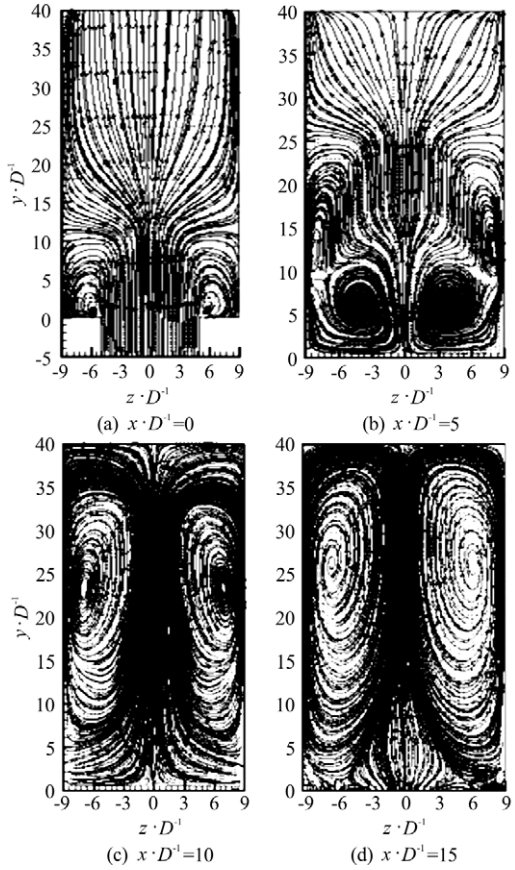


Fig.16 Mean *y-z* vector plots superimposed on streamline at different downstream locations for R = 9, x/D = 0, 5, 10, and 15

The mean velocity field at different *y-z* planes at various x/D locations (x/D = 0, 5, 10, and 15) for the velocity ratio R = 9 is shown in Fig.16. The structures of the flow field at the first two positions (x/D = 0 and 5) are similar to the case of R = 6, but far downstream (x/D = 10 and 15) the structures of the flow field are quite different from those for R = 6. At these two planes, the sizes of the CRVP are elongated. At the plane x/D = 10, the two vortex centers are somewhat far from the central plane (z/D = 0). At further downstream locations (x/D = 15), the vortex centers come closer to the central plane and also move up.

5. Conclusions

A 3-D numerical investigation of the mean flow field of a turbulent rectangular jet in a narrow channel crossflow has been presented in this study using the standard k-ε model. The present investigation

establishes the three-dimensionality of the flow field. The effect of the velocity ratio on the flow field is discussed by considering two values of the velocity ratio R = 6 and 9. The velocity ratio is found to affect the flow features such as the trajectory and the lateral spread of the jet and the low velocity region downstream of the jet. The formations of different types of vortices in the flow field are discussed. The effect of the velocity ratio on the formation of these vortices is also observed. A high value of the velocity ratio is associated with the reduced size of the wake vortices and the reverse flow region downstream of the jet slot. The predicted results are in reasonably good agreement with the experimental data reported in the literature. The present investigation provides a deeper insight into various features of this complex flow field compared to those reported in the literature.

References

[1] KASSIMATIS P. G., BERGELES G. C. and JONES T. V. et al. Numerical investigation of the aerodynamics of the near-slot film cooling [J]. **International Journal for Numerical Methods in Fluids,** 2000, 32: 97-117.

[2] PATHAK M., DEWAN A. and DASS A. K. An assessment of streamline curvature effects on the mixing region of a turbulent plane jet in crossflow [J]. **Applied Mathematical Modeling,** 2005, 29: 711-725.

[3] PATHAK M., DEWAN A. and DASS A. K. Effect of streamline curvature on flow field of a turbulent plane jet in cross flow [J]. **Mechanics Research Communication** 2007, 34: 241-248.

[4] FRIC T. F., ROSHKO A. Vortical structures in the wake of a transverse jet [J]. **Journal of Fluid Mechanics**, 1994, 279: 1-47.

[5] KELSO R. M., LIM T. T. and PERRY A. E. An experimental study of round jets in crossflow [J]. **Journal of Fluid Mechanics**, 1996, 306: 111-144.

[6] LIM T. T., KELSO R. M. and PERRY A. E. A study of a round jet in cross-flow at different velocity ratios[C]. **Proceedings of 11th Australian Fluid Mechanics Conference.** Hobart, Australia: University of Tasmania, 1992.

[7] HUMBER A. J., GRANDMAISON E. W. and POLLARD A. Mixing between a sharp-edged rectangular jet and transverse cross flow [J]. **International Journal of Heat Mass Transfer**, 1993, 36: 4307-4316.

[8] LISCINSKY D. S., TRUE B. and HOLDMAN J. D. Crossflow mixing of noncircular jets[J]. **Journal of Propulsion Power**, 1996, 12: 225-230.

[9] HAVEN B. A., KUROSAKA M. The effect of hole geometry on lift-off behaviour of coolant jets [J]. **AIAA Journal**, 1996, 96-0618.

[10] RAMAPRIAN B. R., HANIU H. Turbulence measurement in plane jets and plumes in cross flow[R]. Technical Report, 266, IIHR, Iowa City, IA, USA: University of Iowa, 1983.

[11] HANIU H., RAMAPRIAN B. R. Studies on two-dimensional curved nonbuoyant jets in cross flow [J]. **ASME Journal of Fluids Engineering**, 1989, 111: 78-86.

[12] VERSTEEG H. K. , MALALASEKERA W. **An introduction to computational fluid dynamics the finite volume method** [M]. Malaysia: Logman, 1996.

[13] PATANKAR S. V. **Numerical heat transfer and fluid flow** [M]. Washington, New York, London: Hemisphere Publishing Corporation, 1980.

[14] HODA A., ACHARYA S. Predictions of a film coolant jet in crossflow with different turbulence models [J]. **ASME Journal of Turbomachinery,** 2000, 122: 558-569.

[15] ANDREOPOULOS J., RODI W. Experimental investigation of jets in a cross-flow[J]. **Journal of Fluid Mechanics**, 1984, 138: 93-127.